J. Fluid Mech. (2003), *vol.* 479, *pp.* 145–154. © 2003 Cambridge University Press
DOI: 10.1017/S0022112002003609 Printed in the United Kingdom

On internal fronts

By F. DIAS[1] AND J.-M. VANDEN-BROECK[2]

[1]Centre de Mathématiques et de Leurs Applications, Ecole Normale Supérieure de Cachan, 61 av. Président Wilson, 94235 Cachan, France

[2]School of Mathematics, University of East Anglia, Norwich NR4 7TJ, UK

(Received 21 October 2002 and in revised form 10 December 2002)

The propagation of nonlinear fronts in a channel flow of two contiguous homogeneous fluids of different densities is considered. Each fluid layer is of finite depth. The study is restricted to steady flows in a frame of reference moving with the front. The full governing equations are integrated numerically. The numerical method is based on boundary integral equation techniques. Although the propagation of waves in two-layer fluids is a classical problem, this is the first time that fronts have been directly computed. The limiting configuration of fronts as their amplitude increases is discussed and shown to depend on whether the front is of elevation or of depression.

1. Introduction

An internal front is a wave motion that can arise in the flow of several contiguous homogeneous fluids of different densities. In the ocean for example, differences in density can be associated with differences in temperature, salinity, or amount of suspension. Internal fronts (also called bores and surges) have been observed in rivers, lakes (Loch Ness for example), fjords (Trondheim fjord for example), oceans (off the coast of California for example), and their profiles can be displayed by echo-sounders. The presence of a sill near the mouth of a river or fjord may be responsible for the formation of an internal bore. This is the case for example in Knight Inlet, British Columbia, and through the Straits of Gibraltar. Internal bores are usually generated in a comparatively thin layer of water which lies above a deeper denser layer, so the front is expected to appear as a wave of depression (Simpson 1997).

The focus of this paper is fronts of permanent form. In a frame of reference moving with it, the front can be viewed as a steady interfacial wave (see figure 1). The flow is uniform upstream and downstream. Here we consider the simplest model with just two layers of different densities bounded above and below by horizontal walls. The velocity of the uniform flow far upstream is assumed to be the same in each layer and is denoted by U. Besides reducing the number of independent parameters of the problem by one, this restriction is needed when dealing with fronts of permanent form travelling downstream into fluids otherwise at rest. The upstream thicknesses of the upper and lower layers are, respectively, h_2 and h_1. In this paper, quantities related to the upper fluid layer are indexed with the subscript 2, while those related to the lower fluid layer are indexed with the subscript 1.

In the absence of an obstacle in the channel, two uniforms flows are said to be conjugate if the following four quantities are all conserved: mass in the bottom fluid layer, mass in the upper layer, total momentum and total energy (Benjamin 1966). In general, for arbitrary values of U, h_1 and h_2, conjugate flows do not exist. The reason is that although there are four conserved quantities leading to four equations

https://doi.org/10.1017/S0022112002003609 Published online by Cambridge University Press

for four unknowns (the heights and the uniform velocities downstream), there is the additional constraint that the total height of the channel is fixed. Let the upstream Froude number be defined by

$$F = \frac{U}{\sqrt{gh_1}}, \tag{1.1}$$

where g is the acceleration due to gravity. The density ratio $\rho = \rho_2/\rho_1$ is assumed to be less than 1 (stable configuration). The thickness ratio h_2/h_1 is denoted by β. It is well-known (see e.g. Laget & Dias 1997 Appendix A) that a necessary condition for fronts to exist is that the square of the upstream Froude number (1.1) equal

$$F^2_{\text{front}} = \frac{(1+\beta)(1-\sqrt{\rho})}{1+\sqrt{\rho}}. \tag{1.2}$$

Moreover fronts necessarily satisfy the following properties:

$$\left(\frac{U_2}{U_1}\right)_{\text{downstream}} = \frac{\beta}{\sqrt{\rho}}, \quad \left(\frac{h_2}{h_1}\right)_{\text{downstream}} = \sqrt{\rho}. \tag{1.3}$$

The value

$$\beta = \sqrt{\rho} \tag{1.4}$$

is a critical value for fronts: if $\beta < \sqrt{\rho}$, the front appears as a wave of depression; if $\beta > \sqrt{\rho}$, the front appears as a wave of elevation. If $\beta = \sqrt{\rho}$, there is no front.

Internal fronts are closely related to internal solitary waves. Such waves have been studied analytically, numerically and experimentally. Amick & Turner (1989) and Mielke (1995) used the centre manifold approach to prove rigorously the existence of small-amplitude solitary waves and fronts. They showed that solitary waves bifurcate from a uniform flow at $F = F_{\text{bifurcation}}$, where

$$F^2_{\text{bifurcation}} = \frac{\beta(1-\rho)}{\beta+\rho}, \tag{1.5}$$

and are characterized by a Froude number larger than $F_{\text{bifurcation}}$. Whether they are of elevation or depression depends on the ratio of layer depths. As for fronts, the bifurcating solitary waves are of depression if $\beta < \sqrt{\rho}$ and of elevation if $\beta > \sqrt{\rho}$. The Froude numbers (1.2) and (1.5) are precisely equal when $\beta = \sqrt{\rho}$. Makarenko (1992) used bifurcation theory to prove the existence of fronts. In addition to these local results, global results have been obtained by Amick & Turner (1986). Their analytical results predict either the broadening or the overhanging of solitary waves as their speed increases but cannot predict which one will occur. The question of how large internal waves can be is of importance for example for oil rig construction in marginal seas. The precise nature of limiting internal solitary waves remains an open problem. Accurate nonlinear interfacial solitary waves (or long periodic waves) have been obtained numerically. Funakoshi & Oikawa (1986) used truncated Fourier expansion series, Turner & Vanden-Broeck (1988) used an integrodifferential equation formulation, Mirie & Pennell (1989) used a ninth-order perturbation expansion, Moni & King (1995) used a generalized Schwarz–Christoffel transformation technique. All these authors provided numerical evidence for broadening of solitary waves, and consequently for fronts since broad solitary waves can be viewed as the superposition of two fronts. Pullin & Grimshaw (1988) and Rusås & Grue (2002) used an integral equation formulation to compute overhanging solitary waves.

Solitary waves have also been observed in laboratory conditions by several authors, including Gavrilov (1994), Maurer, Hutter & Diebels (1996), and Michallet &

https://doi.org/10.1017/S0022112002003609 Published online by Cambridge University Press

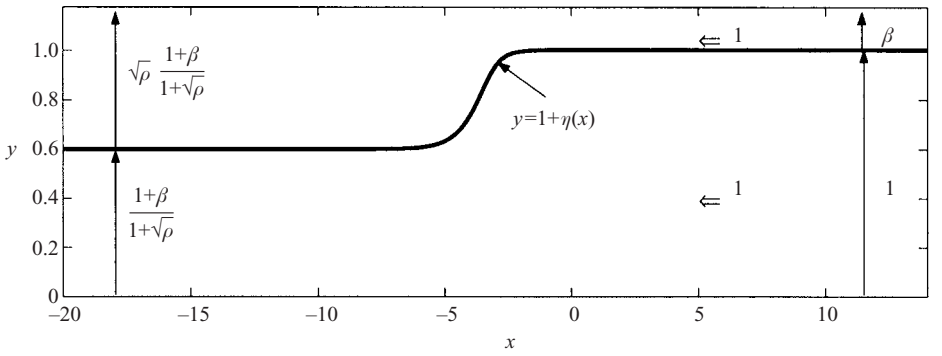


FIGURE 1. Sketch of a depression front in dimensionless coordinates. The densities of the upper and lower fluids are, respectively, ρ_2 and ρ_1. The density ratio $\rho = \rho_2/\rho_1$ is less than 1. The flow is uniform upstream with the same uniform velocity -1 in both layers. The thickness of the bottom layer is 1 upstream and $(1+\beta)/(1+\sqrt{\rho})$ downstream. The thickness of the upper layer is β upstream and $\sqrt{\rho}(1+\beta)/(1+\sqrt{\rho})$ downstream. This is a computed solution with $\beta = 0.175$, $\rho = 0.9$ and F given by (1.2).

Barthélemy (1998). Gavrilov (1994) also mentions laboratory observations of fronts. Although there is analytical, numerical and experimental evidence for fronts, this is the first time that fronts have been directly computed.

2. Formulation

A front travelling from left to right at speed U between two contiguous incompressible inviscid fluids of different densities is considered. The fluids are assumed to be at rest on the right-hand side. The analysis is made in a frame of reference moving with the front so that a uniform velocity $-U$ is superimposed everywhere. The unit of length is the height h_1. The unit of velocity is U and the flow in dimensionless variables is sketched in figure 1. The x-axis is the bottom of the channel. The y-axis is vertical. The flow is uniform far upstream, with the same velocity -1 in both layers.

The flows in each layer are assumed to be potential. In dimensionless form, the governing equations in each layer are

$$\Delta\phi_i = 0\,, \quad i = 1, 2, \tag{2.1}$$

where ϕ_i is the velocity potential in layer i. Along the interface described by $y = 1 + \eta(x)$ there are two kinematic conditions

$$\frac{\partial\phi_i}{\partial x}\frac{\mathrm{d}\eta}{\mathrm{d}x} - \frac{\partial\phi_i}{\partial y} = 0, \quad i = 1, 2. \tag{2.2}$$

Using Bernoulli's equation in each fluid and eliminating the pressure at the interface, one can write the dynamic condition in the form

$$\tfrac{1}{2}|\nabla\phi_1|^2 - \tfrac{1}{2}\rho|\nabla\phi_2|^2 + (1-\rho)\frac{1}{F^2}\eta = \tfrac{1}{2}(1-\rho). \tag{2.3}$$

The condition of no flow normal to the walls is given by

$$\frac{\partial\phi_1}{\partial y} = 0 \ \text{ at } \ y = 0, \quad \frac{\partial\phi_2}{\partial y} = 0 \ \text{ at } \ y = 1+\beta. \tag{2.4}$$

https://doi.org/10.1017/S0022112002003609 Published online by Cambridge University Press

We will show below that fronts form a two-parameter family of solutions, the two parameters being, for example, ρ and β.

3. Linear and weakly nonlinear analysis

Given waves of the form $\phi_1 = -x + \varphi_1$ and $\phi_2 = -x + \varphi_2$, the linearization of (2.1)–(2.4) results in the dispersion relation for infinitesimal waves of wavenumber k:

$$kF^2(\tanh k\beta + \rho \tanh k) = (1-\rho)\tanh k \tanh k\beta. \tag{3.1}$$

Real values for k can be found only if the Froude number (1.1) is less than $F_{\text{bifurcation}}$ (1.5). This paper deals with fronts, which are supercritical solutions ($F_{\text{front}} > F_{\text{bifurcation}}$). Through the transformation $k \to \mathrm{i}\lambda$, equation (3.1) becomes

$$\lambda F^2(\tan \beta\lambda + \rho \tan \lambda) = (1-\rho)\tan \lambda \tan \beta\lambda, \tag{3.2}$$

where λ measures the exponential decay of the front upstream, i.e. the front decays as $\exp(-\lambda x)$ upstream.

Insight into the origin of fronts can be obtained by performing a classical perturbation expansion for long waves ($k \to 0$) on (2.1)–(2.4). Such an expansion leads to the Korteweg–de Vries (KdV) equation. Since the present paper deals with stationary solutions, only the stationary KdV equation is considered. In dimensionless variables, it takes the form

$$\tfrac{1}{6}b\eta_{xxx} + \tfrac{3}{2}a\eta\eta_x - (F - F_{\text{bifurcation}})\eta_x = 0, \tag{3.3}$$

where

$$a = \frac{\beta^2 - \rho}{\beta(\beta+\rho)}F_{\text{bifurcation}}, \quad b = \beta\left(\frac{1+\beta\rho}{\beta+\rho}\right)F_{\text{bifurcation}}. \tag{3.4}$$

The scaling

$$x \to \sqrt{\epsilon}\frac{x}{\sqrt{b}}, \quad \eta \to \frac{1}{\epsilon}|a|\eta, \quad F - F_{\text{bifurcation}} = \epsilon\mu \tag{3.5}$$

transforms (3.3) into

$$\tfrac{1}{6}\eta_{xxx} \pm \tfrac{3}{2}\eta\eta_x - \mu\eta_x = 0, \tag{3.6}$$

where the plus sign is chosen if $\beta > \sqrt{\rho}$ and the minus sign is chosen if $\beta < \sqrt{\rho}$. Integrating equation (3.6) once leads to

$$\eta_{xx} \pm \tfrac{9}{2}\eta^2 - 6\mu\eta = 0, \tag{3.7}$$

under the condition that the flow is uniform far upstream.

Equation (3.7) has two fixed points: $\eta = 0$ and $\eta = \pm\frac{4}{3}\mu$, and its solutions are well-known. Integrating equation (3.7) once leads to

$$\eta_x^2 = 6\mu\eta^2 \mp 3\eta^3 + \text{constant}. \tag{3.8}$$

For $\mu > 0$ (the case of interest in this paper), the solutions are periodic (cnoidal waves) or homoclinic (solitary waves). The solitary waves are of elevation if $\beta > \sqrt{\rho}$ (negative cubic term in (3.8)) and of depression if $\beta < \sqrt{\rho}$ (positive cubic term in (3.8)). Note that (3.6) does not admit fronts.

Near the critical ratio of layer depths (1.4), the coefficient a of the quadratic term $\eta\eta_x$ is small and the cubic term $\eta^2\eta_x$ must be computed. The modified KdV equation takes the form

$$\tfrac{1}{6}b\eta_{xxx} + \tfrac{3}{2}a\eta\eta_x - \tfrac{3}{4}c\eta^2\eta_x - (F - F_{\text{bifurcation}})\eta_x = 0, \tag{3.9}$$

https://doi.org/10.1017/S0022112002003609 Published online by Cambridge University Press

where

$$a = \frac{2(\beta - \sqrt{\rho})}{\sqrt{\rho}(1+\sqrt{\rho})} F_{\text{bifurcation}}, \quad b = (1 - \sqrt{\rho} + \rho) F_{\text{bifurcation}}, \quad c = \frac{4}{\sqrt{\rho}} F_{\text{bifurcation}}. \tag{3.10}$$

The scaling

$$x \to \epsilon \frac{x}{\sqrt{b}}, \quad \eta \to \frac{1}{\epsilon}\sqrt{c}\eta, \quad \frac{a}{\sqrt{c}} = \epsilon e, \quad F - F_{\text{bifurcation}} = \epsilon^2 \mu \tag{3.11}$$

transforms (3.9) into

$$\tfrac{1}{6}\eta_{xxx} + \tfrac{3}{2} e \eta \eta_x - \tfrac{3}{4}\eta^2 \eta_x - \mu \eta_x = 0. \tag{3.12}$$

Integrating (3.12) once leads to

$$\eta_{xx} + \tfrac{9}{2} e \eta^2 - \tfrac{3}{2}\eta^3 - 6\mu\eta = 0, \tag{3.13}$$

under the condition that the flow is uniform far upstream.

Solutions of equation (3.13) are well-known. If $\mu > (9/16)e^2$, it has only one fixed point: $\eta = 0$. If $\mu < (9/16)e^2$, it has three fixed points:

$$\eta = 0, \quad \eta = \tfrac{3}{2}e - \tfrac{1}{2}\sqrt{9e^2 - 16\mu}, \quad \eta = \tfrac{3}{2}e + \tfrac{1}{2}\sqrt{9e^2 - 16\mu}. \tag{3.14}$$

For $\mu > 0$ (the case of interest in this paper), the non-trivial fixed points are positive if $e > 0$ and negative if $e < 0$.

Integrating equation (3.13) once leads to

$$\eta_x^2 = 6\mu\eta^2 - 3e\eta^3 + \tfrac{3}{4}\eta^4 + \text{constant}. \tag{3.15}$$

Solutions of (3.15) depend on μ (that is on $F - F_{\text{bifurcation}}$) and on e (that is on $\beta - \sqrt{\rho}$).

When $\mu > 0$, the fixed point $\eta = 0$ is a saddle point. The middle fixed point is a centre while the third fixed point is a saddle point. When $0 < \mu < \frac{1}{2}e^2$, the bounded solutions are qualitatively similar to those of the KdV equation. When $\mu = \frac{1}{2}e^2$, the only bounded solution going through the origin is a front given by

$$\eta = e\left[1 + \tanh\left(\tfrac{1}{2}\sqrt{3}ex\right)\right]. \tag{3.16}$$

When $\mu > \frac{1}{2}e^2$, there is no bounded solution going through the origin. Note that the value $\mu = \frac{1}{2}e^2$ is equivalent to $F = F_{\text{front}}$ (within the weakly nonlinear approximation). Moreover the amplitude $2|e|$ of the front agrees with the conjugate flow estimates.

A summary of the weakly nonlinear results on the modified KdV equation is as follows. Solitary waves exist for all values of the Froude number between $F_{\text{bifurcation}}$ and F_{front}. They are of depression if $\beta < \sqrt{\rho}$ and of elevation if $\beta > \sqrt{\rho}$. They broaden as the Froude number increases towards F_{front}. When $F = F_{\text{front}}$, solitary waves disappear and are replaced by fronts.

4. Numerical scheme

Our numerical procedure to integrate numerically (2.1)–(2.4) closely follows the work of Sha & Vanden-Broeck (1993) and Dias & Vanden-Broeck (2002). In these two papers, there was an obstacle on the bottom of the channel. Here the procedure is simpler because there is no obstacle.

The interface is described parametrically by $x = X(s)$ and $y = Y(s)$, where s is the arclength. Therefore we require

$$[X'(s)]^2 + [Y'(s)]^2 = 1, \tag{4.1}$$

https://doi.org/10.1017/S0022112002003609 Published online by Cambridge University Press

where primes denote derivatives with respect to s. We choose $s = 0$ at the point $x = 0$, $y = t$ on the interface (i.e. $X(0) = 0$, $Y(0) = t$). Here t is given. Typically we chose $t = \frac{1}{2}[Y(-\infty) + Y(\infty)]$. Equation (2.3) can be rewritten as

$$\tfrac{1}{2}[\phi_1'(s)]^2 - \tfrac{1}{2}\rho[\phi_2'(s)]^2 + (1-\rho)\frac{1}{F^2}(Y(s)-1) = \tfrac{1}{2}(1-\rho). \tag{4.2}$$

Following Sha & Vanden-Broeck (1993), we derive the integral equations

$$-\pi[\phi_2'(s)X'(s) - 1] = \int_{-\infty}^{\infty} \frac{[\phi_2'(\sigma) - X'(\sigma)][Y(\sigma) - Y(s)] + [X(\sigma) - X(s)]Y'(\sigma)}{[X(\sigma) - X(s)]^2 + [Y(\sigma) - Y(s)]^2}\,\mathrm{d}\sigma$$
$$+ \int_{-\infty}^{\infty} \frac{[\phi_2'(\sigma) - X'(\sigma)][Y(\sigma) + Y(s) - 2\beta - 2] + [X(\sigma) - X(s)]Y'(\sigma)}{[X(\sigma) - X(s)]^2 + [2\beta + 2 - Y(\sigma) - Y(s)]^2}\,\mathrm{d}\sigma \tag{4.3}$$

and

$$\pi[\phi_1'(s)X'(s) - 1] = \int_{-\infty}^{\infty} \frac{[\phi_1'(\sigma) - X'(\sigma)][Y(\sigma) - Y(s)] + [X(\sigma) - X(s)]Y'(\sigma)}{[X(\sigma) - X(s)]^2 + [Y(\sigma) - Y(s)]^2}\,\mathrm{d}\sigma$$
$$+ \int_{-\infty}^{\infty} \frac{[\phi_1'(\sigma) - X'(\sigma)][Y(\sigma) + Y(s)] + [X(\sigma) - X(s)]Y'(\sigma)}{[X(\sigma) - X(s)]^2 + [Y(\sigma) + Y(s)]^2}\,\mathrm{d}\sigma. \tag{4.4}$$

We note that (4.3) and (4.4) differ from equations (5) and (8) in Sha & Vanden-Broeck (1993) because we did not assume symmetry with respect to the y-axis.

This concludes the formulation of the problem. We seek ϕ_1', ϕ_2', $X(s)$ and $Y(s)$ so that the four equations (4.1)–(4.4) are satisfied. These equations are discretized by following the procedure outlined in Sha & Vanden-Broeck (1993) and the resulting algebraic equations are solved by Newton iterations. The number of independent parameters for fronts is two. These two parameters are for example ρ and β, or ρ and F.

5. Numerical results

The numerical scheme described in § 4 was used to compute fronts for various values of the parameters. Most of the solutions were obtained with 200 mesh points. The convergence of the scheme and the accuracy of the results were checked by increasing independently the number of mesh points and the size of the computational domain.

5.1. *Depression fronts* ($\beta < \sqrt{\rho}$)

Our numerical computations agree qualitatively with the weakly nonlinear results of § 3. Typical interfacial profiles with $\rho = 0.4$ are shown in figure 2(a) for $\beta = 0.4, 0.2, 0.1$. The value $\rho = 0.4$ was chosen for comparison with existing results on broad solitary waves. A profile with $\rho = 0.9$ is shown in figure 1.

5.2. *Limiting configuration for depression fronts*

The profiles shown in figure 2(a) suggest that in the limit β going to zero (the top layer becoming thinner and thinner) the interface will touch the top wall. This hypothesis was tested numerically by computing directly solutions in which the upstream flow is such that the heavy fluid occupies the whole channel. Such a solution is shown in figure 2(b). There is in fact a one-parameter family of such solutions, the parameter being the Froude number (1.1). But only one is the limiting configuration of the front, the one corresponding to $F = F_{\mathrm{front}}$ with $\beta = 0$. It gives $F = (1 - \sqrt{\rho})^{1/2}/(1 + \sqrt{\rho})^{1/2}$.

https://doi.org/10.1017/S0022112002003609 Published online by Cambridge University Press

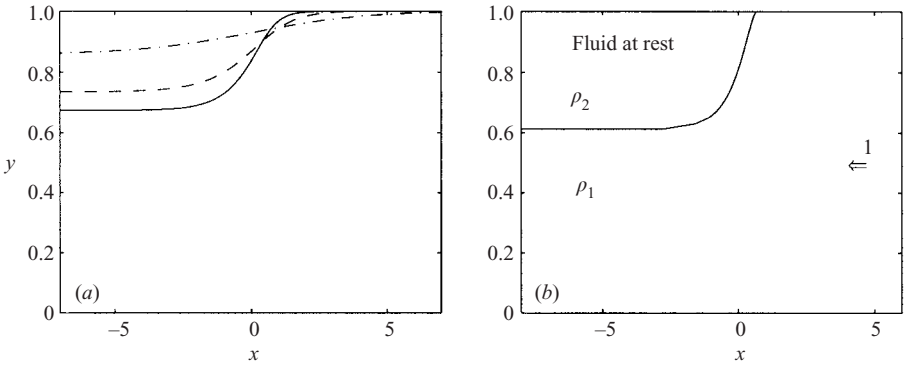


FIGURE 2. Depression fronts with $\rho = 0.4$. (*a*) $\beta = 0.4$ (dash-dotted line), $\beta = 0.2$ (dashed line), $\beta = 0.1$ (solid line). (*b*) Limiting configuration $\beta \to 0$. The bottom lies at $y = 0$ and the top wall at $y = 1 + \beta$. The thickness of the bottom layer is $(1 + \beta)/(1 + \sqrt{\rho})$ downstream.

The governing equations for the velocity potential ϕ_1 are

$$\Delta\phi_1 = 0, \quad \tfrac{1}{2}|\nabla\phi_1|^2 + (1-\rho)\frac{1}{F^2}\eta = \text{constant}. \tag{5.1}$$

The solutions were obtained by the method of series truncation (see for example Dias & Vanden-Broeck 1989). The problem is reformulated here in an intermediate t-plane. The flow domain is mapped onto the upper half-unit disk and the complex velocity is expanded as a Taylor series inside the unit disk. The image of the interface is the upper half-unit disk. The image of the solid boundaries is the real diameter, with $t = -1$ the image of the point where the interface touches the top wall, $t = 0$ the image of infinity upstream and $t = 1$ the image of infinity downstream. Introducing the complex potential f, the mapping is provided by

$$f = \frac{1}{\pi}\log\left[\frac{t}{(1-t)^2}\right]. \tag{5.2}$$

The complex velocity $\zeta = \mathrm{d}f/\mathrm{d}z = u - \mathrm{i}v$, with $z = x + \mathrm{i}y$, is expanded as

$$\zeta = \exp(\Omega(t)), \quad \text{where} \quad \Omega(t) = A(1-t)^{2\lambda/\pi} + \sum_0^\infty a_n t^n. \tag{5.3}$$

The coefficients a_n and the constant A are real. The power λ is the smallest solution of an equation similar to (3.2),

$$\frac{\lambda}{F}\sqrt{1-\rho} = \tan\lambda. \tag{5.4}$$

Parameterizing the interface by $t = \mathrm{e}^{\mathrm{i}\sigma}, 0 \leqslant \sigma \leqslant \pi$, and differentiating Bernoulli's equation in (5.1) with respect to σ leads to

$$uu_\sigma + vv_\sigma - \frac{1}{\pi}\left(\frac{1-\rho}{F^2}\right)\left(\frac{\cos\frac{1}{2}\sigma}{\sin\frac{1}{2}\sigma}\right)\frac{v}{u^2+v^2} = 0. \tag{5.5}$$

This completes the reformulation of the problem. The coefficients a_n in (5.3) are sought such that (5.5) is satisfied on the interface. The problem is solved numerically by truncating the infinite series in (5.3) after $(N-1)$ terms. Next we introduce the N mesh points on the interface $\sigma_I = (I - \frac{1}{2})\pi/N, 1 \leqslant I \leqslant N$. We satisfy equation (5.5) at

https://doi.org/10.1017/S0022112002003609 Published online by Cambridge University Press

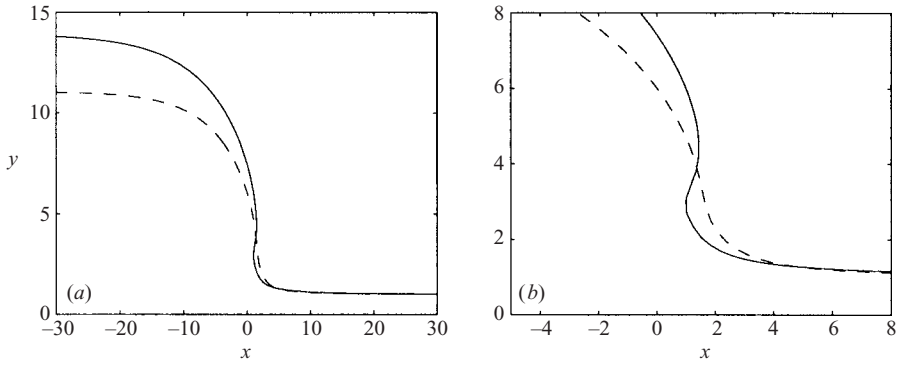


FIGURE 3. Elevation fronts with $\rho = 0.4$. (*a*) $\beta = 17$ (dashed line), $\beta = 21.6$ (solid line). (*b*) Blow up of the overhanging region. The bottom lies at $y = 0$ and the top wall at $y = 1+\beta$. The thickness of the bottom layer is $(1+\beta)/(1+\sqrt{\rho})$ downstream.

the mesh points. This yields N equations for the N unknowns $A, a_0, a_1, \ldots, a_{N-2}$. For given values of F, this system of N nonlinear equations with N unknowns is solved by Newton's method. It can be shown that $\frac{1}{2}\sqrt{1-\rho} < F < \sqrt{1-\rho}$ for solutions to exist (Benjamin 1968). The upper bound corresponds to a uniform flow while the lower bound corresponds to a limiting configuration with a 120° angle (Asavanant & Vanden-Broeck 1996). When $F = F_{\text{front}}$, which is indeed in the admissible range, the solution is the limit of a depression front. This limit is in agreement with the numerical computations of Rusås & Grue (2002) on solitary waves (see their figure 13*b*).

5.3. *Elevation fronts*

Our numerical computations agree qualitatively with the weakly nonlinear results of § 3 for small-amplitude fronts. But for large-amplitude fronts, the interface may be overhanging. Typical profiles with $\rho = 0.4$ are shown in figure 3 for $\beta = 17$ and 21.6.

5.4. *Limiting configuration for elevation fronts*

The profiles shown in figure 3 indicate that the limiting configuration as β tends to infinity (the top layer becomes thicker and thicker) is different from the limiting configuration for depression fronts.

Solutions with the interface touching the bottom wall can be computed but it can be shown that they require $\frac{1}{2}\sqrt{1-\rho}/\sqrt{\rho} < F < \sqrt{1-\rho}/\sqrt{\rho}$. The upper bound corresponds to a uniform flow while the lower bound corresponds to a limiting configuration with a 120° angle. It turns out that F_{front} is not in the admissible range, unless we consider the Boussinesq limit $\rho \to 1$ (see § 5.5). In the Boussinesq limit, $F_{\text{front}}^2/(1-\rho)$ is equal to $\frac{1}{4}(1+\beta)$.

Our numerical computations suggest that as a branch of solutions is followed by fixing ρ and increasing β, a maximum value of β is ultimately reached. This maximum value of β, $\beta_{\max}$, is in fact a turning point and the values of β start to decrease as the branch is extended past the limiting value. The profile for $\beta = 21.6$ in figure 3 is close to $\beta_{\max}$. Our results are in agreement with the numerical computations of Rusås & Grue (2002) on solitary waves (see their figure 11*a*).

5.5. *Boussinesq limit*

Figure 4 shows profiles corresponding to the Boussinesq limit $\rho \to 1$. In that case solutions exist over the whole range $0 < \beta < \infty$ and the solutions for $\beta = 0$ and ∞

https://doi.org/10.1017/S0022112002003609 Published online by Cambridge University Press

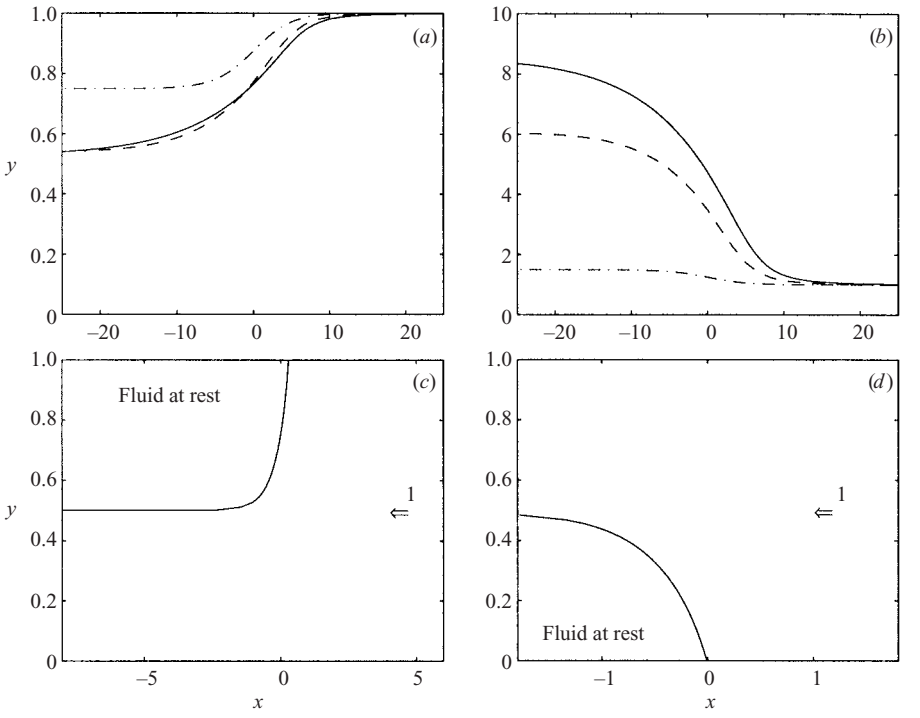


FIGURE 4. Fronts in the Boussinesq limit ($\rho \to 1$). (a) Depression fronts: $\beta = 1/2$ (dash-dotted line), $\beta = 1/11$ (dashed line), $\beta = 1/16$ (solid line). (b) Elevation fronts: $\beta = 2$ (dash-dotted line), $\beta = 11$ (dashed line), $\beta = 16$ (solid line). (c) Limiting depression front. (d) Limiting elevation front. In (a–c), the top wall lies at $y = 1 + \beta$; in (d), the y-coordinate has been rescaled so that the top wall lies at $y = 1$.

touch, respectively, the upper and lower wall. They intersect the walls with a 120° angle.

6. Discussion

The main conclusion is that depression fronts exist for all values of β between 0 and $\sqrt{\rho}$ while elevation fronts exist only for values of β between $\sqrt{\rho}$ and $\beta_{\max}(\rho)$. The limiting configuration of depression fronts is obtained when the interface touches the top wall. The limiting configuration of elevation fronts is not as clear. What is clear is that overhanging develops.

The weakly nonlinear results predict a symmetry of fronts with respect to their centre. The fully nonlinear results clearly show that it is not the case. The fronts we computed cannot be generalized in the sense that no oscillations can appear on the downstream part. Indeed the dispersion relation downstream is (see for example Lamb 1932, art. 234)

$$kU_1^2 \tanh kh_2 + kU_2^2 \rho \tanh kh_1 = g(1-\rho) \tanh kh_1 \tanh kh_2. \tag{6.1}$$

Downstream of the front, U_1, U_2, h_1 and h_2 are known. Plugging these known values into the dispersion relation (6.1) shows that there is no real solution for k. In other words fronts with oscillations on the downstream part are not possible. On the other hand, the stability of fronts is not so easily solved; they are locally subject to

https://doi.org/10.1017/S0022112002003609 Published online by Cambridge University Press

the Kelvin–Helmholtz instability downstream. However it is not known at present whether or not the local instability can destroy the front.

This work was supported in part by EPSRC, the Leverhulme Trust and the National Science Foundation (NSF). J.-M. V.-B. thanks the Centre National de la Recherche Scientifique (CNRS) for sponsoring his visit to Ecole Normale Supérieure de Cachan in 2002.

REFERENCES

Amick, C. J. & Turner, R. E. L. 1986 A global theory of internal solitary waves in two-fluid systems. *Trans. Am. Math. Soc.* **298**, 431–484.

Amick, C. J. & Turner, R. E. L. 1989 Small internal waves in two-fluid systems. *Arch. Rat. Mech. Anal.* **108**, 111–139.

Asavanant, J. & Vanden-Broeck, J.-M. 1996 Nonlinear free-surface flows emerging from vessels and flows under a sluice gate. *J. Australian Math. Soc.* B **38**, 63–86.

Benjamin, T. B. 1966 Internal waves of finite amplitude and permanent form. *J. Fluid Mech.* **25**, 241–270.

Benjamin, T. B. 1968 Gravity currents and related phenomena. *J. Fluid Mech.* **31**, 209–248.

Dias, F. & Vanden-Broeck, J.-M. 1989 Open channel flows with submerged obstructions. *J. Fluid Mech.* **206**, 155–170.

Dias, F. & Vanden-Broeck, J.-M. 2002 Steady two-layer flows over an obstacle. *Phil. Trans. R. Soc. Lond.* A **360**, 2137–2154.

Funakoshi, M. & Oikawa, M. 1986 Long internal waves of large amplitude in a two-layer fluid. *J. Phys. Soc. Japan* **55**, 128–144.

Gavrilov, N. V. 1994 Internal solitary waves and smooth bores which are stationary in a laboratory coordinate system. *J. Appl. Mech. Tech. Phys.* **35**, 29–33.

Laget, O. & Dias, F. 1997 Numerical computation of capillary–gravity interfacial solitary waves. *J. Fluid Mech.* **349**, 221–251.

Lamb, H. 1932 *Hydrodynamics*, 6th edn. Cambridge University Press.

Makarenko, N. I. 1992 Smooth bore in a two-layer fluid. *Intl Ser. Numer. Math.* **106**, 195–204.

Maurer, J., Hutter K. & Diebels S. 1996 Viscous effects in internal waves of two-layered fluids with variable depth. *Eur. J. Mech.* B/*Fluids* **15**, 445–470.

Michallet, H. & Barthélemy, E. 1998 Experimental study of interfacial solitary waves. *J. Fluid Mech.* **366**, 159–177.

Mielke, A. 1995 Homoclinic and heteroclinic solutions in two-phase flow. In *Proc. IUTAM/ISIMM Symp. on Structure and Dynamics of Nonlinear Waves in Fluids*, pp. 353–362. World Scientific.

Mirie, R. M. & Pennell, S. A. 1989 Internal solitary waves in a two-fluid system. *Phys. Fluids* A **1**, 986–991.

Moni, J. N. & King, A. C. 1995 Guided and unguided interfacial solitary waves. *Q. J. Mech. Appl. Maths* **48**, 21–38.

Pullin, D. I. & Grimshaw, R. H. J. 1988 Finite-amplitude solitary waves at the interface between two homogeneous fluids. *Phys. Fluids* **31**, 3550–3559.

Rusås, P.-O. & Grue, J. 2002 Solitary waves and conjugate flows in a three-layer fluid. *Eur. J. Mech.* B/*Fluids* **21**, 185–206.

Sha, H. & Vanden-Broeck, J.-M. 1993 Two-layer flows past a semicircular obstruction. *Phys. Fluids* A **5**, 2661–2668.

Simpson, J. E. 1997 *Gravity Currents*, 2nd edn. Cambridge University Press.

Turner, R. E. L. & Vanden-Broeck, J.-M. 1988 Broadening of interfacial solitary waves. *Phys. Fluids* **31**, 2486–2490.

https://doi.org/10.1017/S0022112002003609 Published online by Cambridge University Press